Applied Acoustics 95 (2015) 50–56

Contents lists available at ScienceDirect

Applied Acoustics

journal homepage: www.elsevier.com/locate/apacoust

Reducing interior noise in a cylinder using micro-perforated panels

Cheng Yang, Li Cheng *, Zhongyu Hu

Department of Mechanical Engineering, The Hong Kong Polytechnic University, Hung Hom, Kowloon, Hong Kong Special Administrative Region

ARTICLE INFO

Article history:
Received 14 November 2014
Received in revised form 9 February 2015
Accepted 10 February 2015

Keywords:
Micro-perforated panel
Cylindrical enclosure
Acoustic coupling

ABSTRACT

Sound absorption inside a cylindrical enclosure using micro-perforated panels (MPP) is investigated. Attention is focused on analyzing the effect of backing cavities on the sound absorption capabilities of various MPP configurations both numerically and experimentally. A model is used to analyze the acoustic coupling between the cylindrical acoustic domain enclosed by the MPP and the annular cylindrical acoustic domain forming the air space behind it. It was shown that the sound field in the backing cavity of the MPP plays an important role in determining the energy dissipation efficiency of the MPP construction, and thereby affects the degree of attenuation of the standing waves inside the enclosure. Conventional MPP construction with a backing air layer was shown to only provide limited noise reduction, but fail at certain frequencies associated with the acoustic resonances of the cylindrical acoustic field. The problem can be tackled by adding proper partitions in the baking cavity, as a result of the alteration of the acoustic coupling across the MPP panels.

1. Introduction

The pioneer work on micro-perforated panel (MPP) can be traced back to nearly forty years ago. By expanding the short tube theory, Maa's work [1] allows the theoretical prediction of the acoustic impedance of a MPP. To achieve effective sound absorption, an air gap is usually placed between the MPP and a backing rigid wall so as to produce the Helmholtz resonance effect. Without considering the panel vibration, the acoustic impedance of the MPP is independent of the material properties. Hence, it can be fabricated by waterproof, heatproof or flameproof materials, making it a good alternative to conventional fibrous and porous materials in numerous acoustic applications [2–15].

Generally speaking, two major parameters are usually used to quantify the acoustic property of a MPP construction: the sound absorption coefficient and the normal acoustic impedance over its surface. With MPP construction placed on a wall, both parameters are widely used by treating the MPP as equivalent acoustic boundaries. Those two quantities, however, may not truthfully represent the *in-situ* working condition of the MPP when it is integrated into a compact acoustic system. Recent work [16] showed that two MPP constructions, one with a partitioned backing air space and the other one without, give the same sound absorption curves in the impedance tube test, but exhibit totally different sound absorption behaviors when placed on the wall of a rectangular enclosure. The work indicated that the acoustic behavior of the MPP could be strongly influenced by the acoustic media coupled across the MPP, which is drastically different from the free field configuration. Indeed, a MPP dissipates acoustic energy through Helmholtz resonance absorption inside the holes, as a result of the pressure difference between the two sides of the MPP. In this sense, how the sound pressure field behind MPP behaves will, in principle, affect the dissipation capability of the MPP. More recently, Toyoda et al. [17] and Yu et al. [18] noticed that even the conventionally used backing air cavity behind the MPP is not always necessary, provided a pressure difference between the two sides of MPP is formed. Despite these observations and hypotheses, thorough analyses which allow clear understanding of the underlying physics are still lacking. This motivates the present work to take a closer look at the MPP construction by undertaking a systematic analysis of the working mechanism of the MPP in the presence of the acoustic coupling across its surface.

As a benchmark problem, the interior sound field inside a cylindrical enclosure with an inner MPP liner is investigated. The MPP liner consists of a folded MPP with various backing configurations. Particular attention is paid to studying different configurations of the backing air space of the MPP liner. Note that the cylindrical enclosure is also of considerable importance in many engineering applications such as aircraft fuselage, ventilation duct and Magnetic Resonance Image (MRI) scanner. It is also relevant to note that in a previous work, Li and Mechefske [19] examined the possibilities of using MPP liner to reduce the noise level in the MRI scanner bore. The backing air space of the MPP is left

* Corresponding author. Tel.: +852 2766 6769.
E-mail address: li.cheng@polyu.edu.hk (L. Cheng).

http://dx.doi.org/10.1016/j.apacoust.2015.02.003
0003-682X/

empty without any particular treatment. Measurements showed that although MPP could reduce the interior noise to some extent, it is not so effective in some cases. A later investigation by Fraser [20] reported that the noise reduction is not sufficient for significant differences in perceptions by volunteers tested in MRI experiment. The present paper will provide an answer to these observed phenomena. As will be demonstrated later, the noise suppression capability of the MPP can be improved with proper treatment to the backing air space. The general understanding of the underlying physics could also assist in improving the noise control performance of MPPs in other applications.

2. Numerical analyses

2.1. Model development

Under a cylindrical coordinate system, an annular cylinder of outer radius $r1$, inner radius $r2$, and length L is shown in Fig. 1. Assuming an acoustically rigid outer wall, the inner cylindrical wall represents a MPP boundary with:

$$v_1 = \frac{p_1 - p_2}{Z_{MPP}} \tag{1}$$

$$v_1 = -v_2 \tag{2}$$

where p_i is the sound pressure on the MPP surface, v_i is the averaged normal air particle velocity over the MPP surface (positive outward), and Z_{MPP} is the acoustic impedance of the MPP given by Maa [1]. Subscript 1 and 2 denote the two acoustic domains, respectively, *i.e.* the one between the two cylindrical walls; and the other enclosed by the inner cylindrical MPP wall. The two terminations of the acoustic domains are assumed to be acoustically rigid.

With a point source inside acoustic domain 2, the air motion inside the MPP pores becomes a secondary source, radiating sound into domains 1 and 2 simultaneously. In harmonic regime, the sound pressure field in domain 2 can be described by the Kirchhoff–Helmholtz integral equation [21] as

$$p_2 = -j\rho\omega \int_{S_a} G_2 v_2 dS_a + \int_{V_s} G_2 Q dV_s \tag{3}$$

where G_2 is the Green's function, Q has the expression of $Q = j\rho\omega q\delta(r - r_s)\delta(x - l_s)$ with ρ, ω, q, $\delta(-)$, r_s, l_s being respectively, the air density, angular frequency, volume velocity of the point source, the Dirac delta function, the radial and longitudinal distances of the point source. r and x are the radial and longitudinal distances of the observing point. S_a is the surface occupied by MPP and V_s is the volume of the point source.

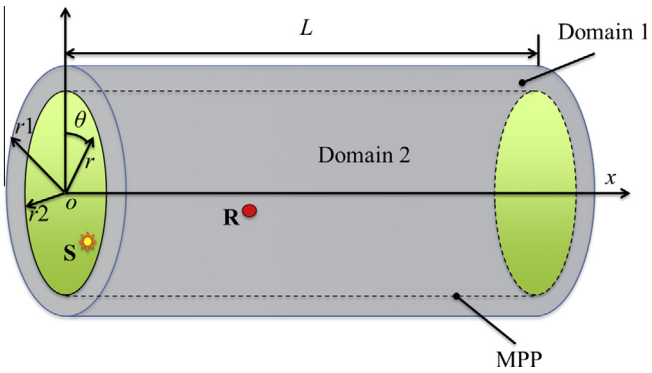

Fig. 1. Diagram for the MPP lined on the inner wall of a cylindrical acoustic domain, a uniform air space of depth $r1 - r2$ is left behind the MPP.

Table 1
Parameters of the cylinder and MPP in simulation.

Cylinder	MPP	
$r1$ = 230 mm	Diameter of the hole	0.35 mm
$r2$ = 200 mm	Panel thickness	0.35 mm
l = 400 mm	Perforation ratio	1%

Similarly, the sound field in domain 1 is also determined by the velocity on MPP surface:

$$p_1 = -j\rho\omega \int_{S_a} G_1 v_1 dS_a \tag{4}$$

The rigid-walled modes of the two domains can be expressed analytically [22–24]. For domain 1 (annular cylindrical cavity), the Mth rigid-walled mode ϕ_M is expressed as:

$$\phi_M(r,x) = \begin{Bmatrix} \cos(m\theta) \\ \sin(m\theta) \end{Bmatrix} * \left(J_m(k_{mn}r) - \frac{J'_m(k_{mn}r2)}{Y'_m(k_{mn}r2)} Y_m(k_{mn}r) \right) * \cos\left(\frac{p\pi x}{L}\right) \tag{5}$$

where k_{mn} is the zero of the cross-product of Bessel function and θ is the azimuthal angle.

$$J'_m(k_{mn}r2)Y'_m(k_{mn}r1) - J'_m(k_{mn}r1)Y'_m(k_{mn}r2) = 0 \tag{6}$$

In Eqs. (5) and (6), J_m and Y_m are the Bessel functions of the first and second kind of order m, respectively; the prime indicates the first derivative; L is the length of the cylinder; m, n, p are the circumferential, radial longitudinal order, respectively.

For domain 2 (cylindrical cavity), the Nth rigid-walled mode ψ_N writes

$$\psi_N = \begin{Bmatrix} \cos(m\theta) \\ sin(m\theta) \end{Bmatrix} * J_m(k_{mn}r) * \cos\left(\frac{p\pi x}{L}\right) \tag{7}$$

where k_{mn} satisfies the following equation

$$J'_m(k_{mn}r2) = 0 \tag{8}$$

The Green's functions G_1 and G_2, which describe the response at (r,x) due to point source excitation at (r',x'), can be constructed by the corresponding rigid-walled modes in each domain as

$$G_1(r,r',x,x') = \sum_M \frac{\phi_M(r,x)\phi_M(r',x')}{\Lambda_{1M}\left(k_{1M}^2 - k^2\right)} \tag{9}$$

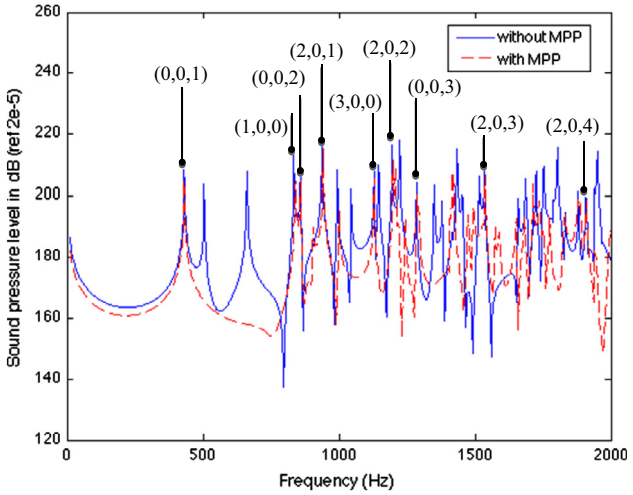

Fig. 2. Simulated interior sound pressure level.

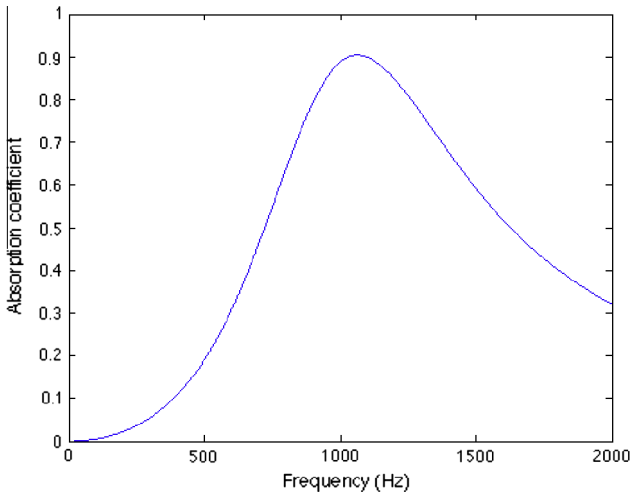

Fig. 3. Sound absorption coefficient curve for the MPP having a backing air layer of depth 30 mm.

$$G_2(r,r',x,x') = \sum_N \frac{\psi_N(r,x)\psi_N(r',x')}{\Lambda_{2N}\left(k_{2N}^2 - k^2\right)} \tag{10}$$

with the modal mass defined as

$$\Lambda_{1M} = \int_{V_1} \phi_M^2(x,r)dV \tag{11}$$

$$\Lambda_{2N} = \int_{V_2} \psi_N^2(r,x)dV \tag{12}$$

With the Green's functions defined in Eqs. (9) and (10), Eqs. (3) and (4) can be solved by substituting them into the boundary conditions in Eqs. (1) and (2), and by using the orthogonal property of the rigid-walled modes with proper modal truncation. Unlike conventional boundary integral method, in which the MPP construction is modeled as an impedance boundary, the model developed here considers the air space behind MPP as a sound field. As will be shown later, such treatment turns out to be necessary, which facilitates the understanding of the influence of the backing sound field to the sound absorption capability of the MPP construction.

2.2. Numerical analyses

The developed model is coded to investigate the effectiveness of MPP construction upon the cylindrical sound field (domain 2). A point source located at $l = 0.02$ m, $r = 0.17$ m, $\theta = 36°$ is adopted to drive the sound field. Geometrical parameters and those of the MPP are listed in Table 1.

The interior sound pressure level without MPP (rigid-walled) and with MPP treatment (MPP lined on the side wall of the original

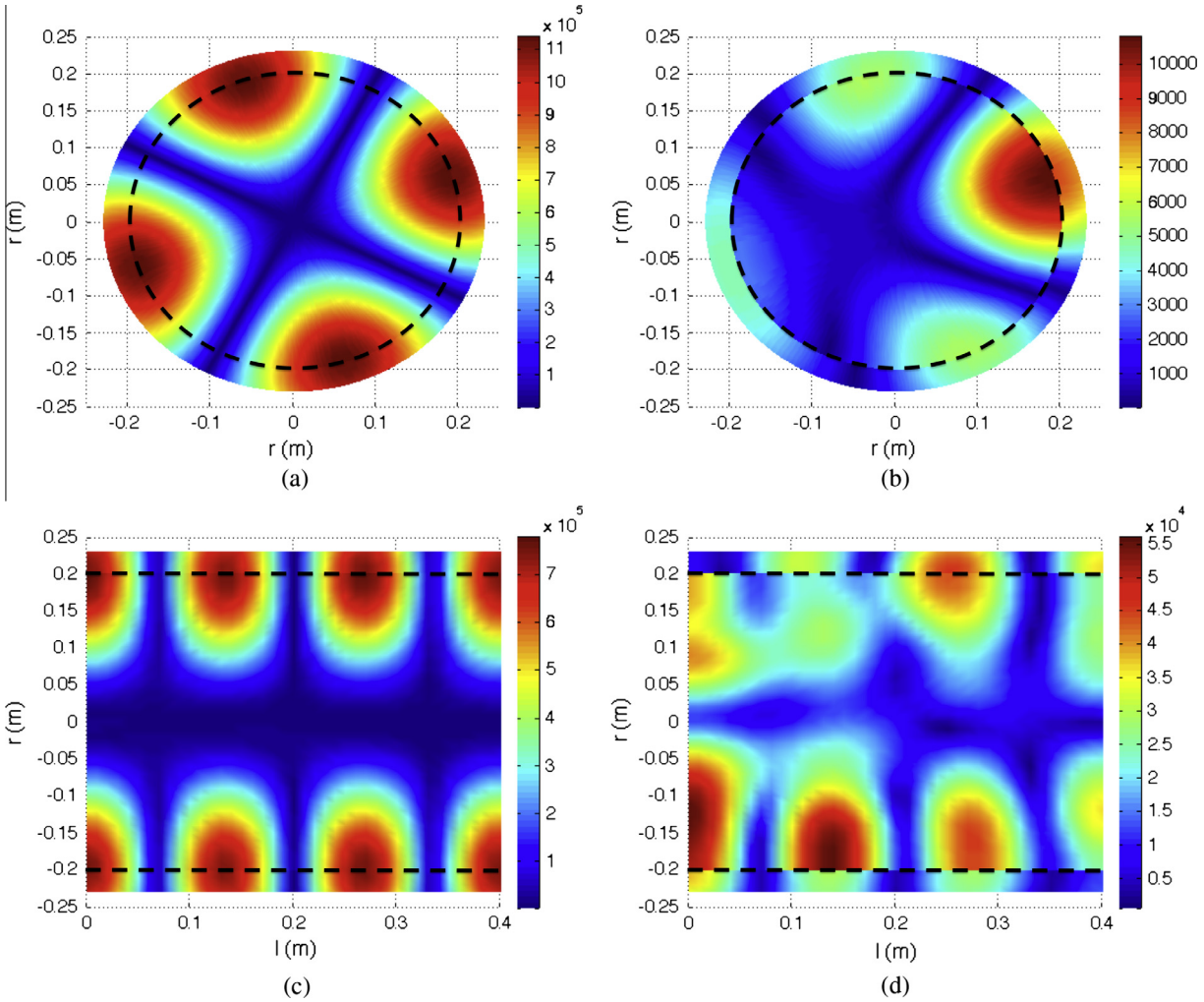

Fig. 4. Cross-sectional view of the sound pressure distribution at different frequencies: (a) 942 Hz, plane normal to the axis $l = 0.3$ m; (b) 1046 Hz, plane normal to the axis at $l = 0.3$ m; (c) 1536 Hz, plane parallel and passing through the axis; (d) 1514 Hz, plane parallel and passing through the axis (dash line: MPP).

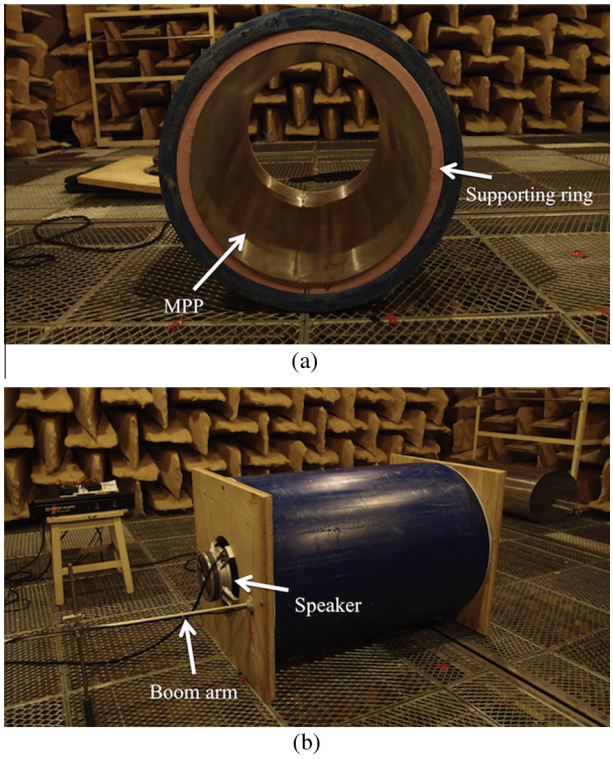

Fig. 5. Experimental setup. (a) Lining MPP over the inner wall of the pipe with an air depth of 30 mm; (b) installation of the loudspeakers.

cylinder with an air space of 30 mm), observed at $l = 0.36$ m, $r = 0.17$ m, $\theta = 90°$, is shown in Fig. 2. As a reference, the sound absorption coefficient curve of the cavity-backed MPP subject to normal plane wave incidence is given in Fig. 3. Comparing the two figures, the broadband absorption indicated by the sound absorption curve is not manifested in terms of the sound pressure reduction in Fig. 2. For example, at the frequencies around the sound absorption peak (Fig. 3), the sound pressure is not significantly suppressed. More specifically, there exist several resonances (denoted by black dots in Fig. 2), whose magnitudes are nearly unaffected. In fact, if one checks these frequencies carefully, they correspond to a class of the resonances of the rigid-walled modes of the cylindrical domain (listed in Fig. 2). In the figure, each mode is identified by (m,n,p), denoting the circumferential, radial and longitudinal modal order, respectively. As shown in Fig. 2, these unaffected resonances belong to the so-called non-radial modes with $n = 0$, all of which have zero radial order.

In order to better understand the underlying physics, the sound pressure distribution at two unaffected resonances is investigated. Choosing 942 Hz as an example, dominated by mode (2,0,1), a cross-sectional view of the sound pressure distribution within the two domains is displayed in Fig. 4(a). It can be seen that the two acoustic domains exhibit the same wave pattern in the circumferential direction. Indeed, by virtue of the coaxiality and the equal length of the two acoustic domains, the sound pressure fields on both sides of MPP are dominated by the modes having the same spatial pattern (same circumferential, longitudinal order or their combinations). In addition, the velocity continuity relation on MPP surface causes the equal modal amplitudes of these dominating modes. Hence, at this frequency, the sound pressures on the two sides of the MPP are equal and in phase everywhere over the MPP surface. Recalling its working mechanism, a MPP dissipates acoustic energy through the oscillation of air inside its holes, as a result of the pressure difference between the two sides of MPP. If the sound pressures on the two sides of MPP are equal and in phase, the air inside holes cannot vibrate and hence no energy dissipation could possibly occur. Therefore, at this frequency, MPP behaves like a rigid wall to the main sound field and the resultant sound pressure level is the same as it is in the rigid-walled case. Similar phenomenon can also be observed at 1536 Hz in Fig. 4(c), at which the sound pressure field is dominated by the longitudinal rigid-walled mode. Remember that the undamped resonances happen at resonant frequencies of the non-radial modes only. If the order of the radial mode is non-zero, MPP will be activated and serves as an absorbing boundary. Fig. 4(b) and (d) present the sound pressure distributions at 1046 Hz and 1514 Hz, corresponding to the (0,1,0) and (1,1,1) mode, respectively, in the absence of the MPP. After installing the MPP, apparently, the wave patterns on each side of the MPP are different, resulting in a sound pressure change across the MPP and consequently a significantly reduced sound pressure level inside the cavity as shown in Fig. 2. It is relevant to note that Fig. 4(b) and (d) show no modal sound pressure distribution, as evidenced by the loss of symmetry in the circumferential (Fig. 4(c)) or longitudinal (Fig. 4(d)) directions. This is also an indication that MPP takes effects and modifies the original modes (before MPP is installed) by coupling the two acoustic media. Since the point source is arbitrarily placed inside the main cavity, the sound distributions shown in Fig. 4(b) and (d) are no longer single-mode dominant and symmetrical.

Table 2
Parameters of the cylinder and the MPP in experiment.

Cylinder		MPP	
Diameter	620 mm	Thickness	0.35 mm
Length	970 mm	Hole diameter	0.35 mm
		Perforation	1%
		Depth of backing air space	30 mm

3. Experimental verifications

3.1. Experimental setup

Numerical analyses show that the sound field behind MPP, in association with the modal feature of the annular cylindrical cavity, plays an important role in determining the dissipation efficiency of MPP. Overlooking the detailed acoustic field behind the MPP could lead to an overestimation of the sound absorption effect of the MPP liner, especially at the frequencies that are dominated

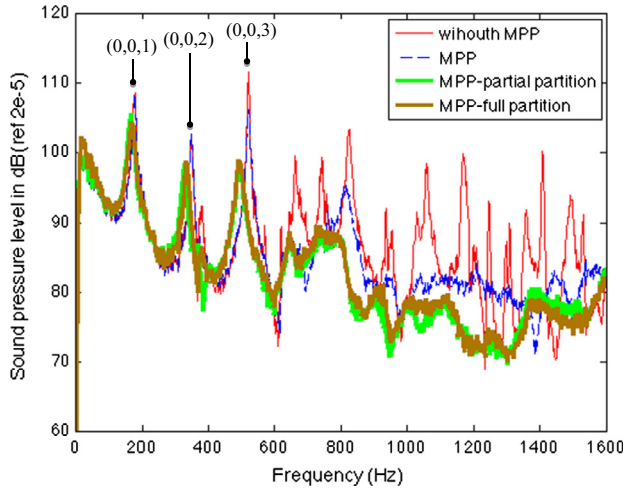

Fig. 6. Measured interior sound pressure level: Symmetric excitation (marker: typical longitudinal modes of the cylinder).

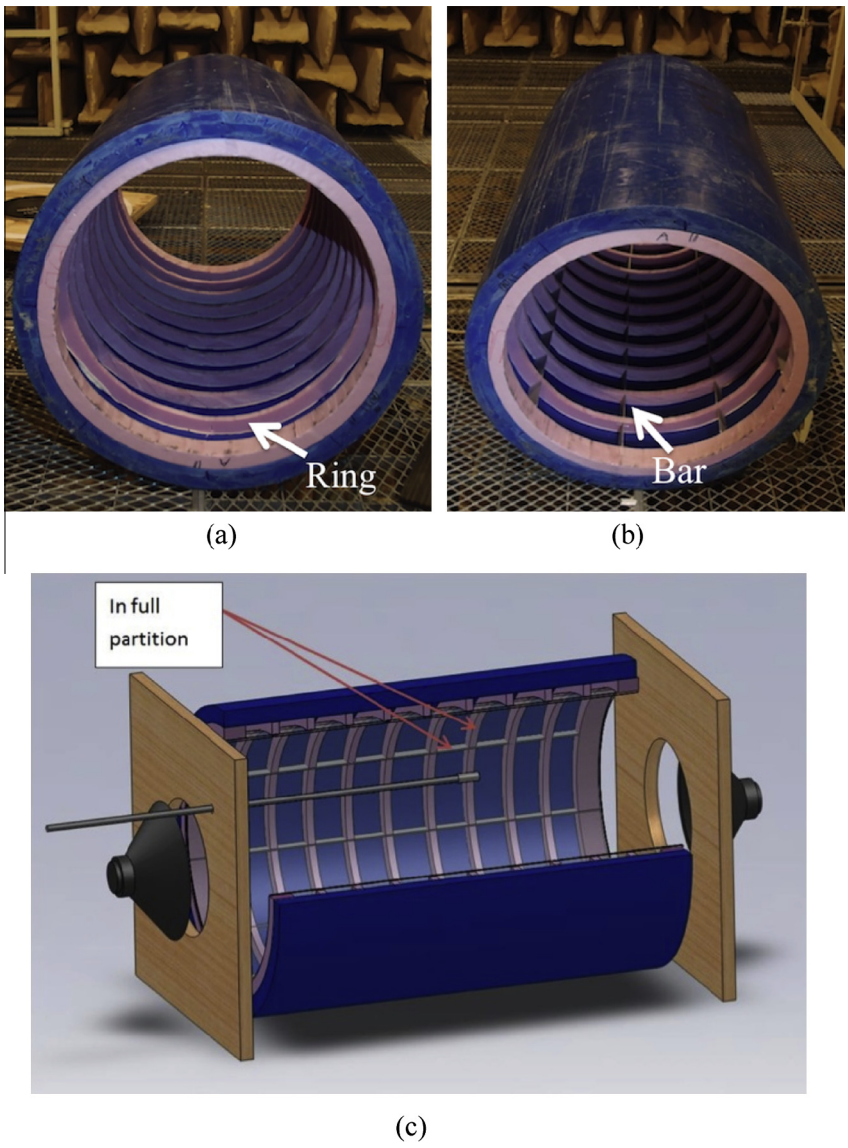

Fig. 7. (a) Installation of rings inside the pipe (partial partition); (b) installation of rings and bars inside the pipe (full partition); (c) CAD drawing of the experimental setup for full partition case (MPP not shown).

by the circumferential and/or the longitudinal modes of the cylindrical cavity. To confirm this observation, two experiments were deliberately designed to identify and to reduce the influence induced by those two types of modes. A PVC water pipe is used to represent the cylinder. The shell has thickness of 30 mm, hard enough to be acoustically rigid. A MPP sheet is wrapped and lined on the inner wall of the pipe. A uniform air space is maintained between the MPP wall and the inner wall of the pipe by placing two thin rings at the two ends of the pipe. Fig. 5(a) shows the installation of the MPP inside the pipe. Two wooden lids are placed at the two ends of the pipe to enclose the cylinder. A loudspeaker was mounted at the center of each wooden lid, each generating a white noise to the enclosure. A B&K 4942 1/2 type microphone is held by a boom arm, placed inside the cylinder through a hole opened on the wooden lid (Fig. 4(b)). Detailed information about the pipe and the MPP are tabulated in Table 2.

The interior sound pressure level, at several points, is measured in two cases, without and with MPP. For the sake of briefness, we show the result of one point only. But the observations apply to other points as well. The coordinate of the observed point is (r = 250 mm, l = 335 mm, θ = 135°), with the origin set on the axis at the left termination of the pipe. The resultant curves are plotted in Fig. 6. For the cylinder without MPP treatment, multiple peaks are observed in the spectrum, associating with the acoustic resonances of the cylindrical domain. When MPP is installed, the sound absorption effect of MPP can be readily visualized, less obvious at low frequencies but more apparent when frequencies increase to 600 Hz, above which multiple resonances are damped due to the presence of the MPP.

3.2. Alteration of longitudinal modes

As far as a cylindrical cavity is concerned, the wave pattern formed in the sound field behind the MPP may possibly deteriorate the dissipation capability of the MPP, and the circumferential and longitudinal modes are identified to be responsible for this degradation in the numerical analysis. To avoid this, the original backing cavity is divided into sub-cavities with partitions installed in two ways: (1). 9 rings are placed behind the MPP to prevent the formation of longitudinal wave pattern in the MPP backing sound field;

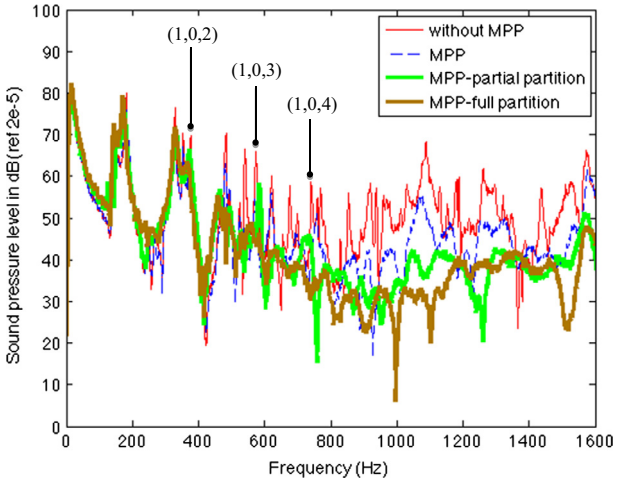

Fig. 8. Measured interior sound pressure level: Non-symmetric excitation (marker: typical circumferential modes of the cylinder).

(2). each annular cylindrical cavity between a pair of rings is further partitioned by 9 bars. The latter treatment is intended to prevent the formation of circumferential wave pattern. The two partitioning treatments are shown in Fig. 7(a) and (b), respectively. For convenience, the first treatment is referred to as partial partition and the second treatment is termed as full partition. A CAD drawing of the experimental setup for the full partition case is displayed in Fig. 7(c).

The interior sound field is measured again for those two new cases, with results displayed in Fig. 6. It can be seen that further sound reduction (compared to the non-partitioned case in Fig. 6 is achieved by partitioning the original backing cavity. A broadband reduction of the sound pressure is visualized above 800 Hz. As a matter of fact, the noise reduction after installing the partitions can be readily perceived by ears during the measurement. The effect of partitions on the longitudinal modes could be more clearly observed at the first three resonant frequencies, which correspond to the first three longitudinal modes of the system. With no partition, these three resonances are nearly unaffected by the MPP liner, in agreement with the observation reported in the numerical analyses. When partitions are introduced, however, these three resonances are reduced and slightly shifted, due to the destruction of longitudinal modes in the annular cylindrical cavity. It is relevant to note that, despite of the improvement on the interior sound field, the two partitioning treatments are found to provide roughly the same control performance. This is caused by the symmetric acoustic source that the loudspeakers provided. In fact, the loudspeakers installed coaxially to the pipe could only effectively activate the longitudinal modes, but not the circumferential ones, thus neutralizing the effect of the partitions along the circumferential direction. This will be further demonstrated in the next section. In brief, as a rule of thumb, if the acoustic excitation is symmetric with respect to the axis of the cylinder, partial partition would be sufficient for improving the sound absorption of the MPP construction.

3.3. Alteration of circumferential modes

The influence of the circumferential modes was not demonstrated due to the symmetric acoustic excitation used in the first design scenario. According to the numerical analyses, it is expected that, with a non-symmetrical excitation, the sound absorption provided by the full partition treatment should outperform the partial partition treatment. To validate this, a point source is used inside the enclosure. The point source is realized by a cone design [16], which consists of a loudspeaker mounted on the base of a cone cabinet. The acoustic energy feeding the small aperture at the top of the cone is concentrated and radiates into the cylindrical domain through a small opening on the wooden pad. The sound pressure level inside the cylindrical enclosure for a point acoustic excitation is measured again for the four cases, with the results given in Fig. 8. It can be seen, partial partition treatment presents better noise control performance than the non-partition treatment. When the full partition treatment is installed, an overall best noise control performance is obtained. Compared with the symmetric acoustic excitation case, the non-symmetric acoustic excitation effectively activates both the longitudinal and circumferential modes in the annular cylindrical cavity. The full partition treatment successfully destructs both types of modes, responsible for the deterioration of the energy dissipation efficiency of the MPP. In more general cases where the acoustic environment inside the enclosure is either non-symmetrical or difficult to be predicted, a MPP liner with fully partitioned backing cavity is preferred.

4. Conclusions

Numerical analyses show that the wave pattern formed in the backing sound field of a MPP construction could significantly influence the dissipation efficiency of a MPP liner inside a cylindrical enclosure through an interaction with the sound field in front of MPP. As a result, the sound absorption coefficient curve measured in the impedance tube cannot truly reflect the *in-situ* sound absorption capability of the MPP construction in the real enclosure configuration, and may even lead to erroneous and overestimated noise reduction prediction. Among all the inherent modes in a cylindrical acoustic system, the longitudinal and circumferential modes are found to be responsible for the deterioration, due to the geometric similarity of the main acoustic domain and the MPP backing acoustic domain. Two experiments are deliberately designed to identify and reduce the influences of these two types of modes by introducing suitable partitions in the backing cavity. The added partitions break up the spatial matching between the acoustic modes on both side of the MPP, thus promoting more effective energy dissipation of the MPP.

Acknowledgements

The authors wish to acknowledge two grants from the Research Grants Council of Hong Kong Special Administrative Region, China (Grants PolyU 5103/13E).

References

[1] Maa DY. Theory and design of microperforated panel sound absorbing constructions. Sci Sin 1975;18(1):55–71.
[2] Kang J, Brocklesby MW. Feasibility of applying micro-perforated absorbers in acoustic window systems. Appl Acoust 2005;66(6):669–89.
[3] Fenech B, Keith GM, Jacobsen F. The use of microperforated plates to attenuate cavity resonances. J Acoust Soc Am 2006;120(4):1851–8.
[4] Asdrubali F, Pispola G. Properties of transparent sound-absorbing panels for use in noise barriers. J Acoust Soc Am 2007;121(1):214–21.
[5] Lee YY, Lee EWM. Widening the sound absorption bandwidths of flexible micro-perforated curved absorbers using structural and acoustic esonances. Int J Mech Sci 2007;49(8):925–34.
[6] Sakagami K, Morimoto M, Yairi M, Minemura A. A pilot study on improving the absorptivity of a thick microperforated panel absorber. Appl Acoust 2008;69(2):179–82.
[7] Cobo P, Ruiz H, Alvarez J. Double-layer microperforated panel/porous absorber as liner for anechoic closing of the test section in wind tunnels. Acta Acoust United Acoust 2010;96(5):914–22.
[8] Liu J, Herrin DW. Enhancing micro-perforated panel attenuation by partitioning the adjoining cavity. Appl Acoust 2010;71(2):120–7.
[9] Alexander J, Reed D, Gerdes R. Random incidence absorption and transmission loss testing and modeling of microperforated composites (No. 2011-01-1626). SAE Tech Paper 2011.

[10] Park SH. A design method of micro-perforated panel absorber at high sound pressure environment in launcher fairings. J Sound Vib 2013;332(3):521–35.
[11] Yang C, Cheng L, Pan J. Absorption of oblique incidence sound by a finite micro-perforated panel absorber. J Acoust Soc Am 2013;133:201.
[12] Liu J, Hua X, Herrin DW. Estimation of effective parameters for microperforated panel absorbers and applications. Appl Acoust 2014;75:86–93.
[13] Ortiz S, Gonzalez C, Cobo P, Montero de Espinosa F. Attenuating open cavity tones by lining its walls with microperforated panels. Noise Control Eng J 2014;62(3):145–51.
[14] Putra A, Ismail AY. Normal incidence of sound transmission loss from perforated plates with micro and macro size holes. Adv Acoust Vib 2014.
[15] Sakagami K, Fukutani Y, Yairi M, Morimoto M. A theoretical study on the effect of a permeable membrane in the air cavity of a double-leaf microperforated panel space sound absorber. Appl Acoust 2014;79:104–9.
[16] Yang C, Cheng L. Micro-perforated panel absorber in small-scale cavity. ICSV 21, Beijing.
[17] Toyoda M, Kobatake S, Sakagami K. Numerical analyses of the sound absorption of three-dimensional MPP space sound absorbers. Appl Acoust 2014;79:69–74.
[18] Yu X, Cheng L, Guyader JL. Vibroacoustic modeling of cascade panels system involving apertures and micro-perforated elements. ICSV 21, Beijing; 2014.
[19] Li G, Mechefske CK. A comprehensive experimental study of micro-perforated panel acoustic absorbers in MRI scanners. Magn Reson Mater Phys, Biol Med 2010;23(3):177–85.
[20] Fraser R. Reducing the effects of MRI acoustic noise using micro-perforated panels. MSc thesis, Queen's University; 2012.
[21] Fahy F, Gardonio P. Sound and structural vibration: radiation, transmission and response. Academic press; 2007 [chap 7.3].
[22] Gottlieb HPW. Harmonic properties of the annular membrane. J Acoust Soc Am 1979;66(3):647–50.
[23] Cheng L, Nicolas J. Radiation of sound into a cylindrical enclosure from a point-driven end plate with general boundary conditions. J Acoust Soc Am 1992;91(3):1504–13.
[24] Cheng L. Fluid–structural coupling of a plate-ended cylindrical shell: vibration and internal sound field. J Sound Vib 1994;174(5):641–54.